PCCP

Molecular structure and infrared spectra of dimethyl malonate: A combined quantum chemical and matrix-isolation spectroscopic study†

Susy Lopes,[a] Leszek Lapinski[ab] and Rui Fausto*[a]

[a] Department of Chemistry (CQC), University of Coimbra, P-3004-535, Coimbra, Portugal.
  E-mail: rfausto@ci.uc.pt
[b] Institute of Physics, Polish Academy of Sciences, PL-02-668, Warsaw, Poland

The infrared spectra of dimethyl malonate isolated in low-temperature argon and xenon matrices were studied. Theoretical calculations, carried out at the MP4/6-31G**, MP2/6-31++G** and DFT(B3LYP)/6-311++G** levels, predict two different conformers of nearly equal internal energy, both exhibiting the methyl ester moieties in the *cis* (C–O) configuration. One of the conformers has C_2 symmetry with the two ester groups crossed symmetrically with respect to the C–C–C plane. This structure is doubly degenerated by symmetry. The other form (*gauche*) belongs to the C_1 point group. Four identical-by-symmetry minima on the PES correspond to this structure. The energy of this form is predicted (at the MP4 level) to be slightly lower than that of the C_2 conformer. The six minima on the PES can be divided into two groups of three (one C_2 isomer and two C_1 forms in a group). Each structure from one group is related to its counterpart from the other group by the operation of reflection in the C–C–C plane. In each group, the conformers are separated by low energy barriers (less than 2 kJ mol^{-1}), while conformational interconversions between the two groups imply a transition state structure with a *vis-à-vis* orientation of oxygen atoms and thus are associated with considerably higher energy barriers. The infrared spectra of the matrix isolated compound were found to closely match the spectrum predicted for the C_1 conformer. Annealing of the matrices up to 55 K does not lead to significant changes in the spectra, suggesting that the low energy barriers separating the two conformers allow practically all molecules of dimethyl malonate to transform to the more stable *gauche* conformer, when they are cooled down after landing on the matrix surface. Spectra of the low temperature solid form of the compound (8 K < T < 200 K) also reveal only the presence of the C_1 conformer.

Introduction

Dimethyl malonate (CH$_3$OOCCH$_2$COOCH$_3$, DMM) is one of the simplest, symmetric, saturated dialkyl ester molecules and represents an ideal example of a double-internal-rotor. The molecule consists of two COOMe ester groups that are connected to the central carbon atom by single C–C bonds. The ester groups behave as planar, nearly rigid fragments adopting the *cis*-ester orientation (C–O–C=O dihedral equal to 0°). The energy barrier for interconversion between the low energy *cis* isomers of carboxylic esters, by rotation of the ester group towards a *trans* orientation (C–O–C=O dihedral equal to 180°), is well known to be high (30–50 kJ mol^{-1}) and, in general, these latter conformers are not observed experimentally since the *trans–cis* energy difference is usually larger than 20 kJ mol^{-1}.[1–6]

DMM receives continuously increasing interest because of its practical application. The compound is currently used in the perfume and cosmetic industries. A large group of applications of DMM concerns its role as a reagent in organic chemistry, in particular in asymmetric synthesis. Indeed, malonic esters, in particular dimethyl malonate (DMM) and diethyl malonate, have such numerous applications in organic

synthesis, that it is hard to overestimate their importance. Two properties of malonic esters are mainly exploited in organic reactions. Firstly, these compounds easily undergo decarboxylation, which gives many possibilities for the synthesis of monocarboxylic acids (derivatives of acetic acid).[7,8] Secondly, the protons at the central carbon atom (in the α position with respect to both C=O groups) are labile. The acidic character of the α hydrogen atoms is a consequence of the vicinity of the two electron withdrawing ester groups. The labile proton can be shifted to one of the C=O groups giving rise to the enol tautomer.[9] The proton can also dissociate, leading to a carbanion at the central carbon atom. Hence, a vast number of carbanion reactions known to organic chemistry can be planned and carried out with malonic ester as the starting material.[7] Among them, let us only mention Michael condensation (which is itself a huge class of organic reactions)[8,10,11] and most of the reactions known from the chemistry of β-diketones and β-ketoesters.[12–14]

However, in spite of both fundamental interest and the practical applications of DMM, the available structural and spectroscopic information for this molecule is very scarce. In fact, to the best of our knowledge, only a few studies dealing with the measurement of the dipole moment of DMM in the solution state, together with other carboxylic esters, have been published.[15,16] In the more structurally oriented study of Pitea *et al.*,[17] the dipole moments and Kerr constants were experimentally measured for DMM (among other carboxylic esters) dissolved in tetrachloromethane. The experimental data

---

† Electronic supplementary information (ESI) available: definition of internal symmetry coordinates used in the normal mode analysis of the conformers of dimethyl malonate. See http://www.rsc.org/suppdata/cp/b2/b206270b/

DOI: 10.1039/b206270b

were interpreted based on the assumption of two butterfly-type conformational states of nearly equal energy (where the O=C–C–C dihedrals are 90°/90° and 90°/270°). The height of the energy barrier separating those two forms was predicted as 8–12 kJ mol⁻¹. In that study, theoretical support was obtained from low level CNDO semiempirical calculations. The rigid rotor approximation was applied with the geometrical parameters transferred from methyl acetate.

In the present work the low-energy conformations of DMM were studied by the contemporary theoretical methods of quantum chemistry and by low-temperature matrix-isolation infrared spectroscopy. The potential energy surface of DMM was scanned as a function of the O=C–C–C dihedrals and the lowest energy minima characterized structurally and spectroscopically. The transition state structures for the preferred conformational interconversion reaction pathways were also identified, yielding the energy barriers associated with those processes. Finally, the matrix isolation infrared spectra of DMM in both argon and xenon matrices were obtained and analysed on the basis of comparison with the spectra theoretically predicted at the DFT(B3LYP)/6-311++G** level and with annealing experiments.

Experimental

Dimethyl malonate used in the present study was prepared by acid-catalyzed esterification of malonic acid, as described elsewhere.[18]

The sample of DMM was placed in a glass tube kept at melting ice temperature and vapours of the compound were introduced into the cryostat chamber through a needle valve. DMM was deposited together with a large excess of the matrix gas (argon 99.9999%, or xenon 99.995%, both from Air Liquide) onto the cold CsI window ($T = 8$ K) mounted on the cold tip of the APD Cryogenics DE-202A closed-cycle helium refrigerator. Care was taken to keep the guest to host ratio in the matrices low enough to avoid association. Traces of matrix-isolated methanol impurity were observed in some of the matrices. The very weak bands due to this molecule are easily picked up by comparison with reference data[19] and were later subtracted from the spectra.

The solid amorphous layer of DMM was prepared in the same manner as the matrices, but with the flux of the matrix gas cut off. The layer was then allowed to anneal at a slowly increasing temperature, up to 200 K. Infrared spectra were collected during this process every 20 K of temperature change. After the temperature exceeded 200 K, the substrate was cooled back to 8 K and the final spectrum was recorded.

The IR spectra of the matrices were recorded with a resolution 0.5 cm⁻¹, on a Mattson FTIR spectrometer (Infinity 60AR). In the case of the solid film the resolution was 1.0 cm⁻¹. A SiC global source, a KBr beamsplitter and a DTGS mid-IR detector were used in these measurements.

Computational

Molecular geometries were optimized at the DFT(B3LYP)/6-311++G** and MP2/6-31++G** levels of theory.[20–26] Energies of the two conformers of DMM were also calculated at the MP4/6-31G** level using the previously optimized geometries at the MP2 level. Harmonic wavenumbers were calculated, at the DFT optimized geometries, using the same theoretical method. All the calculations were carried out using the GAUSSIAN 98 program package.[27]

Transformations of the harmonic force constant matrices in Cartesian coordinates to the molecule-fixed internal coordinates allowed for ordinary normal-coordinate analysis to be performed, as described by Schachtschneider.[28] The list of
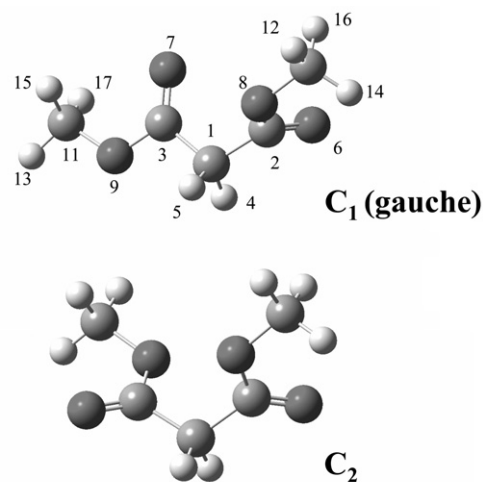

Fig. 1 Structure of the most stable conformers of DMM and atom numbering scheme.

symmetry-adopted internal coordinates used in this analysis is given in the electronic supplementary material, Table S1† (for the atom numbering see Fig. 1). The complete list of calculated frequencies and intensities is provided in Table 1 together with the calculated elements of the potential energy distribution (PED) matrices[29] greater than 10%. In order to correct for vibrational anharmonicity, basis set truncation and the neglected part of the electron correlation, the calculated DFT wavenumbers were scaled down by a single scale factor of 0.97.

Results and discussion

As mentioned in the Introduction, the molecule of DMM consists of two COOMe ester groups connected to the central carbon atom by single C–C bonds. Previous studies of the structures and flexibility of methyl esters[4,30,31] have shown that in COOMe groups the methoxy fragments always adopt the *cis*-ester orientation, while the *trans*-ester orientation is higher in energy by 30 kJ mol⁻¹ or more. Within the methoxy groups, the two out-of-the-COO-plane hydrogen atoms point symmetrically towards the C=O oxygen atom. This is the rule for all simple ester molecules studied so far and the theoretical geometry optimizations carried out in the present work for dimethyl malonate led to the same, usual orientation of atoms in the ester groups. Moreover, previous studies[30,31] show that the non-hydrogen atom skeleton of an ester group can be treated as a rigid unit with the COOC atoms practically coplanar. Hence, the problem of possible DMM conformations can be reduced to consideration of the dihedral angles between the two COO planes of the ester units and the plane of the central CCC atoms.

The theoretical calculations carried out in the present work predict (both at DFT and MP2 levels) two types of low energy minima on the potential energy hypersurface of the studied molecule. The structures corresponding to these minima are presented in a perspective view (Fig. 1) and in a projection onto a plane perpendicular to the C_2–C_3 axis (Fig. 2). One of the minima has C_2 symmetry, with two ester groups crossed symmetrically (with respect to the $C_2C_1C_3$ plane), while the other (*gauche*) minimum has no symmetry, belonging to the C_1 point group. The relative energies of the two minima were calculated to be very similar whatever the level of theory (DFT, MP2, MP4) and basis set used. The results of the calculations of the energies of the C_2 and *gauche* conformations are summarized in Table 2. The sign of the energy difference between the two forms changes as a function of the applied

Table 1 Calculated (scaled, DFT(B3LYP)/6-311++G**) frequencies (ν/cm^{-1}), IR intensities (I^{IR}/km mol^{-1}) and potential energy distributions (PED (%)) for the two most stable conformers of dimethyl malonate

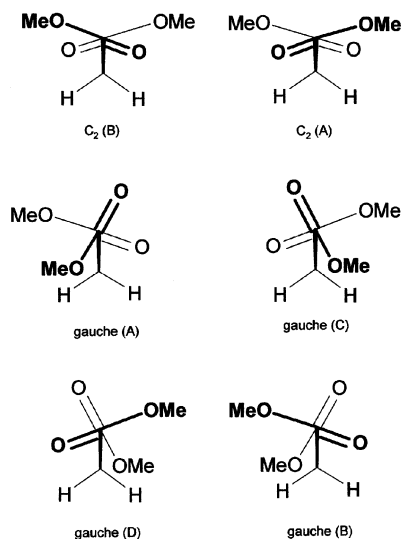| C_1 (gauche)				C_2			
Approximate description	ν_{calc}	I_{calc}	PED	Approximate description	ν_{calc}	I_{calc}	PED
νCH$_3'$ (2)	3066.4	12.3	νCH$_3'$ (2) **(98)**	νCH$_3$ asym (2)	3066.2	15.6	νCH$_3$ asym (2) **(98)**
νCH$_3'$ (1)	3065.8	12.6	νCH$_3'$ (1) **(98)**	νCH$_3$ asym (1)	3066.2	7.1	νCH$_3$ asym (1) **(97)**
νCH$_3''$ (1)	3034.4	16.2	νCH$_3''$ (1) **(98)**	νCH$_2$ asym	3037.0	1.4	νCH$_2$ asym **(100)**
νCH$_3''$ (2)	3034.3	17.3	νCH$_3''$ (2) **(98)**	νCH$_3$ asym$'$ (1)	3033.4	14.3	νCH$_3$ asym$'$ (1) **(100)**
νC–H (1)	3028.8	0.3	νC–H (1) **(64)**, νC–H (2) **(36)**	νCH$_3$ asym$'$ (2)	3033.2	20.1	νCH$_3$ asym$'$ (2) **(100)**
νC–H (2)	2981.2	1.4	νC–H (2) **(64)**, νC–H (1) **(36)**	νCH$_2$ sym	2987.0	0.2	νCH$_2$ sym **(100)**
νCH$_3$ (2)	2962.0	14.0	νCH$_3$ (2) **(78)**, νCH$_3$ (1) **(20)**	νCH$_3$ sym (1)	2961.7	20.9	νCH$_3$ sym (1) **(98)**
νCH$_3$ (1)	2961.7	43.7	νCH$_3$ (1) **(78)**, νCH$_3$ (2) **(20)**	νCH$_3$ sym (2)	2961.3	36.1	νCH$_3$ sym (2) **(98)**
νC=O (1)	1757.2	298.8	νC=O (1) **(51)**, νC=O (2) **(37)**	νC=O sym	1756.5	59.8	νC=O sym **(88)**
νC=O (2)	1740.6	241.2	νC=O (2) **(51)**, νC=O (1) **(37)**	νC=O asym	1736.0	594.2	νC=O asym **(89)**
δCH$_3'$ (2)	1452.6	10.4	δCH$_3'$ (2) **(82)**	δCH$_3$ asym (1)	1452.9	8.1	δCH$_3$ asym (1) **(82)**
δCH$_3'$ (1)	1451.1	9.1	δCH$_3'$ (1) **(83)**	δCH$_3$ asym (2)	1452.6	12.5	δCH$_3$ asym (2) **(82)**
δCH$_3''$ (2)	1439.4	11.3	δCH$_3''$ (2) **(75)**, δCH$_3''$ (1) **(18)**	δCH$_3$ asym$'$ (1)	1439.6	7.9	δCH$_3$ asym$'$ (1) **(93)**
δCH$_3''$ (1)	1439.3	8.6	δCH$_3''$ (1) **(75)**, δCH$_3''$ (2) **(18)**	δCH$_3$ asym$'$ (2)	1439.4	10.4	δCH$_3$ asym$'$ (2) **(93)**
δCH$_3$ (1)	1427.7	19.7	δCH$_3$ (1) **(84)**	δCH$_3$ sym (1)	1427.0	10.4	δCH$_3$ sym (1) **(88)**
δCH$_3$ (2)	1426.3	15.2	δCH$_3$ (2) **(88)**	δCH$_3$ sym (2)	1425.4	16.0	δCH$_3$ sym (2) **(89)**
δCH$_2$	1407.2	24.1	δCH$_2$ **(91)**	δCH$_2$	1410.7	13.2	δCH$_2$ **(98)**
ωCH$_2$	1313.3	212.1	ωCH$_2$ **(60)**, νC–C (2) **(11)**	ωCH$_2$	1279.6	23.4	ωCH$_2$ **(81)**, νC–C asym **(11)**
νC–O (1)	1258.6	136.0	νC–O (1) **(30)**, tw CH$_2$ **(26)**, νC–C (1) **(10)**	νC–O sym	1274.5	237.6	νC–O sym **(32)**, twCH$_2$ **(30)**, νC–C sym **(13)**, δOCO sym **(11)**
νC–O (2)	1179.4	174.6	γCH$_3$ (2) **(43)**, νC–O (2) **(25)**	νC–O asym	1198.6	367.0	νC–O asym **(46)**, νC–C asym **(16)**
γCH$_3$ (1)	1172.6	6.7	γCH$_3$ (1) **(70)**	γCH$_3$ sym	1171.0	5.4	γCH$_3$ sym **(77)**, δCH$_3$ asym (1) **(11)**
γCH$_3$ (2)	1161.7	92.5	γCH$_3$ (2) **(28)**, twCH$_2$ **(24)**, νC–O (2) **(11)**	γCH$_3$ asym	1168.5	19.6	γCH$_3$ asym **(69)**
γCH$_3'$ (1)	1137.5	112.5	γCH$_3'$ (1) **(40)**, γCH$_3'$ (2) **(20)**	twCH$_2$	1145.9	138.9	twCH$_2$ **(60)**, νC–O sym **(15)**
γCH$_3'$ (2)	1136.3	9.2	γCH$_3'$ (2) **(53)**, γCH$_3'$ (1) **(37)**	γCH$_3'$ asym	1136.5	1.6	γCH$_3'$ asym **(92)**
twCH$_2$	1134.2	197.6	twCH$_2$ **(22)**, γCH$_3'$ (2) **(19)**, γCH$_3'$ (1) **(14)**	γCH$_3'$ sym	1136.4	1.6	γCH$_3'$ sym **(91)**
νC–O(CH$_3$)(1)	1014.8	66.0	νC–O(CH$_3$) (1) **(57)**, νC–C (1) **(12)**	νC–O(CH$_3$)asym	1013.8	66.1	νC–O(CH$_3$) asym **(68)**, γCH$_2$ **(11)**
νC–O(CH$_3$)(2)	981.5	15.0	νC–O(CH$_3$) (2) **(55)**, νC–C (2) **(11)**	νC–O(CH$_3$) sym	1005.0	29.2	νC–O(CH$_3$) sym **(69)**, νC–C sym **(13)**
γCH$_2$	932.4	2.6	γCH$_2$ **(33)**, νC–C (1) **(14)**, γC=O (2) **(12)**, νC–O(CH$_3$) (2) **(11)**	νC–C asym	940.0	2.6	γCH$_2$ **(36)**, νC–C asym **(25)**, γC=O asym **(11)**
νC–C (2)	890.3	12.0	νC–C (2) **(23)**, νC–O (2) **(15)**, γC=O (1) **(11)**	γCH$_2$	834.9	31.1	**νC–O asym** (40), **νC–O(CH$_3$) asym** (19), γCH$_2$(13)
νC–C (1)	837.2	13.0	νC–O (1) **(38)**, νC–O(CH$_3$) (1) **(18)**, νC–C (1) **(10)**	νC–C sym	828.6	1.7	νC–O sym **(42)**, νC–O(CH$_3$) sym **(13)**, νC–C sym **(11)**
δOCO (2)	767.2	11.5	γC=O (1) **(30)**, νC–O (2) **(18)**, δOCO (2) **(14)**	γC=O sym	786.6	0.008	γC=O sym **(44)**, δOCO sym **(19)**, δCCC **(15)**
δOCO (1)	670.8	8.6	δOCO (1) **(33)**, δOCO (2) **(16)**, νC–C (1) **(13)**	δOCO asym	672.3	10.8	δOCO asym **(50)**, νC–C asym **(18)**, δCOC asym **(12)**
γC=O (1)	585.4	12.8	γC=O (1) **(35)**, νC–C (2) **(22)**, δOCO (2) **(17)**	γC=O asym	605.4	13.8	γC=O asym **(70)**, γCH$_2$ **(14)**
γC=O (2)	573.7	8.9	γC=O (2) **(67)**, γCH$_2$ **(21)**	δOCO sym	546.4	6.4	νC–C sym **(31)**, γC=O sym **(25)**, δOCO sym **(18)**
δCC=O (2)	396.5	7.5	δCC=O (2) **(57)**, γCH$_2$ **(12)**, δCOC (1) **(11)**	δCC=O sym	400.3	3.2	δCC=O sym **(53)**, νC–C sym **(16)**, δOCO sym **(16)**
δCC=O (1)	354.6	6.8	δCOC (2) **(34)**, δCC=O (1) **(31)**, νC–C (1) **(11)**	δCC=O asym	383.3	7.0	δCC=O asym **(56)**, δCOC asym **(22)**, γCH$_2$ **(12)**
δCOC (1)	278.2	18.3	δCOC (1) **(34)**, δCOC (2) **(18)**, δOCO (2) **(14)**	δCOC sym	288.3	16.4	δCOC sym **(62)**, δCCC **(12)**
δCOC (2)	258.5	9.3	δCOC (1) **(24)**, δOCO (1) **(18)**, δCC=O (2) **(13)**, δCOC (2) **(11)**	δCOC asym	263.4	16.7	δCOC asym **(52)**, δOCO asym **(21)**, δCC=O asym **(20)**
τC–O (1)	196.7	3.4	τC–O (1) **(54)**, δCC=O (1) **(16)**, δCCC **(13)**	τC–O sym	188.4	1.7	τC–O sym **(54)**, δCC=O **(14)**
τC–O (2)	158.6	5.1	τC–O (2) **(86)**, τCH$_3$ (2) **(16)**	τC–O asym	165.6	6.0	τC–O asym **(82)**, τCH$_3$ asym **(14)**
τCH$_3$ (1)	124.2	0.06	τCH$_3$ (1) **(87)**	τCH$_3$ sym	128.3	0.2	τCH$_3$ sym **(92)**
τCH$_3$ (2)	120.8	0.8	τCH$_3$ (2) **(82)**, τC–O (2) **(16)**	τCH$_3$ asym	126.3	0.8	τCH$_3$ asym **(85)**, τC–O asym **(13)**
δCCC	90.6	1.2	δCCC **(37)**, τC–O (1) **(37)**	δCCC	81.3	0.003	δCCC **(45)**, τC–O sym **(36)**, δCC=O sym **(11)**
τC–C (1)	55.9	2.7	τC–C (1) **(73)**, τC–C (2) **(18)**	τC–C sym	44.5	2.4	τC–C sym **(97)**
τC–C (2)	20.6	0.9	τC–C (2) **(87)**, τC–C (1) **(17)**	τC–C asym	21.3	1.6	τC–C asym **(93)**

Fig. 2 Schematic representation of the 6 minima in the potential energy surface of DMM that correspond to its most stable conformers. The structures are presented as projections onto a plane perpendicular to the C_2–C_3 axis. Bold lines and fonts represent the ester group above the plane.

Fig. 3 Cartesian map of the intersecting plane in the potential energy hypersurface of DMM, defined by the torsional coordinates $O_7 = C_3$–C_1–C_2 and $O_6 = C_2$–C_1–C_3. The six minima [four *gauche*, denoted by *gauche* (A to D), and two C_2 (A or B) equivalent-by-symmetry forms - ■] and the transition state (TSn, blue circles) structures between these forms are marked in the map. Red circles are planar *vis-à-vis* oxygen/oxygen crossing structures. Meaning of the connecting lines: Orange: low barriers path between *gauche*(A), C_2(B) and *gauche*(D). Purple: low barriers path between *gauche*(B), C_2(A) and *gauche*(C). Black: symmetry lines of the graph. They do not represent reaction paths. Green: Limits of the unit cell of the graph. The top and left-hand lines are dashed since they are repetitions of the bottom and right-hand lines, and then they do not belong to the same unit cell. Red: reaction paths interconnecting the two low barriers paths. This interconnection may occur: (A) through the C_2 of one path and the *gauche* forms of the other (crossing TS1 or TS2 = TS7 with energy 4.6 kJ mol^{-1} above the global minimum); (B) through *gauche* forms (A and C or B and D). In the latter case, TS4 is involved, whose energy is 6.0 kJ mol^{-1} above that of the global minimum.

method, though, as mentioned above, all the calculations predict the energies of the two forms as nearly equal. A slightly lower energy for the C_2 form is predicted at the DFT/6-31G** and MP2 levels. However, the *gauche* form was calculated as the conformational ground state when the highest (among the applied methods) MP4 level, corrected for the zero point vibrational energy, was used, as well as when the larger 6-311++G** basis set was used in the DFT calculations (see Table 2).

Keeping the $C_2 C_1 C_3$ plane fixed in space, the transformation of the C_2 conformer into the *gauche* form is approximately equivalent to the concerted torsion of the two ester units by 120° (see Fig. 2). An analogous rotation by *ca.* 240° leads to the second *gauche* minimum. Hence, one C_2 and two identical-by-symmetry *gauche* minima can be generated by a concerted rotation of the planes of the two ester units (with $C_2 C_1 C_3$ plane kept fixed in space). The barriers for this type of rotation (and conversion from one form to the other) are low. The barrier height for transformation of the C_2 conformation into one of the *gauche* forms is 1.5 kJ mol^{-1}, while the barrier separating the two *gauche* forms is 1.8 kJ mol^{-1} high.

For each of the three conformations described above, an identical-by-symmetry counterpart, being its mirror image, can be generated (see Fig. 2). The only possibility of transformation of any form presented in the right side of Fig. 2 to any conformation presented in the left side of this figure is by crossing a structure with a *vis-à-vis* orientation of oxygen atoms. The transition structures with such an orientation are comparatively high in energy. The reason for this is the repulsion of the lone electron pairs of the oxygen atoms.

Summarizing, there are six low-energy minima on the potential energy hypersurface of DMM. Two of them are of C_2 symmetry while the four *gauche* minima have no symmetry (C_1 point group). Hence, the *gauche* structure is additionally more probable due to the statistics, the ratio of the statistical weights
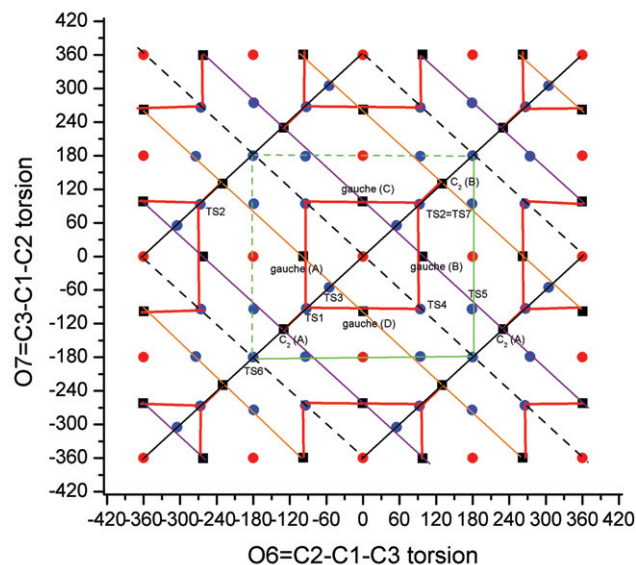
of the C_2 and *gauche* conformers is 1 : 2. The representation of the six minima as well as the barrier peaks (transition states) between them is given in Fig. 3 as a function of two dihedral angles $O_7 = C_3$–C_1–C_2 and $O_6 = C_2$–C_1–C_3. The symmetry relations between the minima and between the transition states are clearly seen in this representation. The values of the energies at the transition states TS1–TS7 (see Fig. 3) between the minima, are collected in Table 3. As shown in this table, the transition state TS6 for a direct conversion from a C_2 form into the second C_2 structure that is its mirror image is particularly high in energy. This transition state corresponds to a pairwise *vis-à-vis* orientation of oxygen atoms, in which the repulsion of lone electron pairs is maximal.

The infrared spectra of dimethyl malonate isolated in Ar and Xe matrices are presented in Fig. 4. These experimental spectra are compared with the spectra theoretically predicted for the C_2 and *gauche* isomers of the compound. The frequencies and intensities of the experimentally observed bands are collected in Table 4, together with the corresponding theoretical (scaled) values. This comparison clearly shows that the experimental spectra of DMM are accurately reproduced by the spectrum calculated for the *gauche* conformer. This is

Table 2 Theoretically calculated relative energies (kJ mol^{-1}) of the two lowest energy conformers of dimethyl malonate

	DFT$^{(6-31G**)}$	MP2$^{(6-31G**)}$	MP2$^{(6-31++G**)}$	MP4$^{(6-31G**)}$	DFT$^{(6-311++G**)}$
$\Delta E_{(C_2\text{-gauche})}$	−0.47	−0.96	−1.16	−0.29	0.48
$\Delta E_{(C_2\text{-gauche})} + \Delta ZPE_{(C_2\text{-gauche})}$	−0.10	−0.59	−0.79	0.08	0.75

Table 3 DFT(B3LYP)/6-311++G** calculated energies (E, kJ mol^{-1}) and relative energies to the conformational ground state (ΔE) of the transition state structures (TSn) for interconversion between the six low energy minima in the potential energy hypersurface of dimethyl malonate

	Minima		Transition state structures						
	Gauche	C_2	TS1: C_2 (A) → g (A)	TS2: g (A) → g (B)	TS3: g (A) → g (D)	TS4: g (D) → g (B)	TS5: C_2 (A) → g (B)	TS6: C_2 (A) → C_2 (B)	TS7 = TS2 g (B) → g (A)
E	−1 303 329.04	−1 303 328.56	−1 303 324.40	−1 303 324.40	−1 303 327.20	−1 303 323.02	−1 303 327.55	−1 303 306.81	−1 303 324.40
ΔE	0.00	0.48	4.64	4.64	1.84	6.02	1.49	22.23	4.64
E+ZPE	−1 302 980.78	−1 302 980.03							
ΔE+ΔZPE	0.00	0.75							

especially clear in the lower (below 1100 cm^{-1}) frequency range, where the anharmonic effects like overtones, combination tones or Fermi resonances are less probable. In this region, there is practically a one to one correspondence between the bands in the experimental and theoretical spectra. Also the region 1800–1750 cm^{-1} in the experimental spectrum is well reproduced by the theoretical calculations carried out for the *gauche* conformer. The absorptions in this range are due to the stretching vibrations of the two C=O groups. In the C_2 conformer these vibrations are coupled (because of symmetry), and the antisymmetric vibration should correspond to a strong IR absorption, while the symmetric vibration should give rise to a weak IR band (see Table 1). In the *gauche* conformer the bands due to the stretching vibrations of the two C=O groups are predicted to have comparable IR intensities. It is noteworthy that the experimental spectra of DMM isolated in Ar and Xe matrices exactly match this last picture. Indeed, even the magnitude of the spacing between the two νC=O bands (13 cm^{-1} Ar; 15 cm^{-1} Xe) is well predicted by the DFT calculations (17 cm^{-1}).

The population of the C_2 conformer in low-temperature matrices must be very low or non-existent. Detection of small amounts of the C_2 form in the presence of the most abundant *gauche* conformer is not easy. In the region below 1100 cm^{-1}

the spectra are not so densely spaced, so the bands due to the, hypothetically present, minor form could be more easily noticed. Unfortunately, in this spectral region all the stronger bands predicted for the C_2 isomer nearly coincide in frequency with bands of the *gauche* form. Nevertheless, small features seen at 843.3 and 689.0 cm^{-1} (Xe) could be considered as candidates for bands from the spectrum of the C_2 form. We have checked that these features do not disappear upon annealing up to 55 K (Xe matrix). With a barrier between the two forms as low as 1.5 kJ mol^{-1} a clear thermally induced interconversion should be expected. That should occur already at temperatures much lower than 55 K. In our recent study of dimethyl fumarate[31] a clear transformation of less stable conformers to the most stable form was observed in an annealing process, though the barriers in that compound should be much higher (30 kJ mol^{-1}). However, no clear transformation of one conformer of DMM to the other occurred upon warming the Xe matrix to 55 K. Minor changes in the spectra can be attributed to site effects, which can be pronounced for a molecule as flexible as DMM.

All the above data suggest that the low barrier between the C_2 and *gauche* forms allowed practically all molecules of DMM to transform to the more stable *gauche* conformer when they were cooled down after landing on the matrix surface.
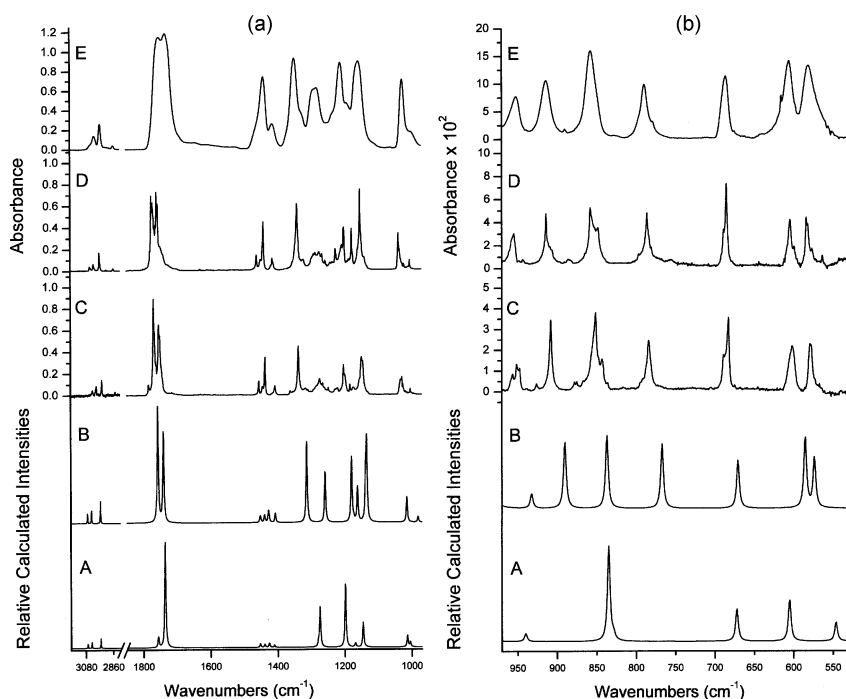

Fig. 4 Infrared spectra of DMM: A, calculated spectrum of conformer C_2; B, calculated spectrum of conformer *gauche*; C, experimental spectrum of the compound isolated in an Xe matrix, D, experimental spectrum of the compound in an Ar matrix. E, experimental spectrum of the solid film (deposited at 8 K, annealed at 200 K and re-cooled to 8 K). Theoretical spectra were calculated at the DFT(B3LYP)/6-311++G** level and scaled down by a factor of 0.97. After annealing of the Xe matrix to 55 K no relevant changes could be observed in the spectra. (a) Higher frequency range; (b) lower frequency range.

Table 4 Observed and calculated (scaled, DFT (B3LYP)/6-311++G**) frequencies and intensities for the C_1 (*gauche*) form of DMM in Ar and Xe matrices and in the solid film

Approximate description	Observed						Calculated	
	Ar		Xe		Solid film		C_1(*gauche*)	
	ν_{exp}	$I_{exp}{}^a$	ν_{exp}	I_{exp}	ν_{exp}	I_{exp}	ν_{calc}	I_{calc}
$\nu CH_3'$ (2)	3044.4	w	3022.4	w			3066.4	12.3
$\nu CH_3'$ (1)							3065.8	12.6
$\nu CH_3''$ (1)	3013.3		2991.8	m	3005.2	m	3034.4	16.2
$\nu CH_3''$ (2)							3034.3	17.3
$\nu C–H$ (2)	2986.4	w					2981.2	1.4
νCH_3 (2)	2966.1	w	2948.0	m	2958.8	S	2962.0	14.0
νCH_3 (1)							2961.7	43.7
$2 \times \delta CH_3'$ (2)	2919.1	w						
$2 \times \delta CH_3''$ (2)	2910.9	w						
$2 \times \delta CH_2$	2853.0	w			2853.4	w		
$\nu C=O$ (1)	1778.8	m	1784.0	m	1750.9	S		298.8
	1774.7	S	1768.9	S			1757.2	
	1770.7	S	1766.6	S				
	1765.2	S	1762.1	S				
$\nu C=O$ (2)	1762.2	S	1753.4	S	1732.2	S		241.2
	1759.3	S					1740.6	
	1755.5	S	1750.3	S				
$\delta CH_3'$ (2)	1461.5	m	1455.1	m			1452.6	10.4
$\delta CH_3'$ (1)							1451.1	9.1
$\delta CH_3''$ (2)	1449.8	m	1444.6	m			1439.4	11.3
$\delta CH_3''$ (1)							1439.3	8.6
δCH_3 (1)	1443.4	sh	1437.4	m	1440.0	S	1427.7	19.7
δCH_3 (2)	1440.7	S	1436.2	S			1426.3	15.2
δCH_2	1414.6	m	1407.3	m	1413.3	S	1407.2	24.1
	1412.5	m						
ωCH_2	1354.7	w	1361.9	w				212.1
	1346.7	sh	1353.7	w				
	1340.5	S	1337.5	S	1347.9	S	1313.3	
	1329.6	m	1316.8	w				
	1325.0	m	1309.2	w	1329.2	sh		
	1321.5	m	1302.6	w				
$\nu C–O$ (1)	1298.3	m						136.0
	1295.0	m	1292.8	w	1289.5	S		
	1291.0	m	1283.5	m				
	1286.3	m					1258.6	
	1274.8	m	1274.4	m				
	1266.6	m	1265.1	m	1279.8	S		
	1256.3	m	1248.2	w				
	1252.4	w						
$\nu C–O$ (2)	1242.0	w	1228.5	w				174.6
	1235.5	w	1223.5	w				
	1226.4	m	1219.9	w	1233.2	sh		
	1224.6	sh	1202.7	S			1179.4	
	1206.1	S	1199.3	m	1210.4	S		
	1200.5	S	1193.8	w				
γCH_3 (1)	1186.2	m	1188.4	w	1191.5	sh	1172.6	6.7
	1182.3	m	1183.6	m				
γCH_3 (2)	1177.6	S	1173.9	w			1161.7	92.5
	1176.0	sh						
$\gamma CH_3'$ (1)	1159.5	S	1154.7	m	1157.0	S	1137.5	112.5
$\gamma CH_3'$ (2)							1136.3	9.2
$tw CH_2$	1152.8	S	1149.5	S				197.6
	1142.9	m	1146.4				1134.2	
	1141.1	m	1146.4	S				
$\nu C–O(CH_3)$ (1)	1038.8	S	1031.6	m				66.0
	1034.8	m	1028.7	m	1027.6	S		
	1027.7	w	1025.4	m			1014.8	
	1021.2	w	1018.0	w				
$\nu C–O(CH_3)$ (2)			1015.6	w			981.5	15.0
	1009.5	w	1013.8	w				
			1009.4	w	998.9	sh		
	1005.4	m	1003.4	w				
			993.6	m				

Table 4 (continued)

Approximate description	Observed						Calculated	
	Ar		Xe		Solid film		C_1(gauche)	
	ν_{exp}	$I_{exp}{}^a$	ν_{exp}	I_{exp}	ν_{exp}	I_{exp}	ν_{calc}	I_{calc}
γCH_2	954.6	w	956.6	w	951.7	w	932.4	2.6
			951.3	w				
	948.7	w	947.6	w				
$\nu C–C$ (2)	913.6	w	908.1	w	914.0	m	890.3	12.0
	908.6	w			890.4	m		
$\nu C–C$ (1)	857.7	w	851.3	w	857.3	m	837.2	13.0
	849.8	w	847.6	w				
	848.0	w	843.3	w				
δOCO (2)	786.0	w	784.0	w	789.4	m	767.2	11.5
	783.5	w						
	780.5	w			779.1	w		
δOCO (1)	688.7	w	689.0	w	686.3	m	670.8	8.6
	685.2	w	682.7	w				
$\gamma C=O$ (1)	604.4	w	615.8	w	615.6	m	585.4	12.8
	599.1	w	602.0	w	605.6	m		
$\gamma C=O$ (2)	582.0	w	579.5	w	581.4	m	573.7	8.9
	581.8	w						
	576.5	w	577.7	w				
$\delta CC=O$ (2)	415.1	w	413.2	w			396.5	7.5
			411.3	w				

^{a} Intensities are presented qualitatively: S, strong, m, medium, w, weak, sh, shoulder.

Before the molecules cool to the surrounding temperature (8 K), the thermal energy, which they still possess, might be enough to cross the low barrier and adopt the lowest energy *gauche* structure. In such a case, the population ratio observed in matrices should correspond nearly to that of the low-temperature equilibrium. Several cases of molecules with such behaviour are known.[32,33] Only one conformer of ethanol was observed in the Ar matrix, though two minima were theoretically predicted for this compound and could afterwards be effectively trapped in N_2 matrices, where specific interactions stabilize the gas-phase higher energy conformer.[33]

The spectrum of the solid film of DMM (vitreous state), obtained by deposition of the gaseous compound (at room temperature) onto the CsI substrate of the cryostat kept at 8 K also reveals the exclusive (or largely dominant) presence of the *gauche* conformer in the sample (see Fig. 4). Hence, efficient conformational cooling could be attained in this case as well. Annealing of the sample to 200 K and subsequent re-cooling to 8 K did not lead to significant changes in the spectrum. Indeed, the glass to crystalline state transition should occur at a higher temperature, which is not accessible under our experimental conditions, since the physical and optical properties of the solid condensate start to deteriorate rapidly at a temperature slightly above 200 K.

As mentioned in the Introduction, one of the most relevant structural peculiarities of DMM, which has been widely demonstrated experimentally,[7–14] is the acidity of its methylene hydrogen atoms leading to easy formation of carbanionic species. The methylene hydrogen atoms in DMM must then be unusually stripped of electrons. Accordingly, the calculated Mulliken charges on these atoms (≈ 0.23 e) are predicted to be almost twice those calculated at the same level of theory (and with the same basis set) for the methylene hydrogen atoms in propane (0.12 e), thus giving further support to this hypothesis.

Conclusion

By a combined use of matrix-isolation infrared spectroscopy and quantum chemistry calculations, undertaken at various levels of theory, it was possible to map the relevant features of the potential energy surface region of DMM (position of the low energy minima and of the transition states associated with the preferred conformational interconversion pathways) and characterize both structurally and spectroscopically the DMM ground conformational state: the fourthly degenerated-by-symmetry *gauche* conformer. A second conformational state, with a slightly higher energy than the *gauche* form, was also predicted by the calculations, corresponding to a doubly degenerated-by-symmetry conformer belonging to the C_2 symmetry point group. The energy barrier for conversion of the C_2 into the *gauche* form was calculated to be less than 1.5 kJ mol^{-1} in the gaseous phase. In consonance with this result, efficient conformational cooling was found to occur during deposition of the vapours of the compound onto the cold substrate of the cryostat. Indeed, the *gauche* form was found to contribute exclusively (or dominantly) to the observed spectra of both the matrix-isolated compound and the low temperature glassy state. Full assignment of the observed spectra was then undertaken, based on the theoretically predicted spectrum for the *gauche* form.

In addition, the positive charges on the methylene hydrogen atoms were obtained and found to be nearly twice those of the methylene hydrogen atoms in propane, confirming the postulated unusual positive charge of DMM methylene hydrogens.

Acknowledgements

References

1 E. M. S. Maçôas, R. Fausto, J. Lundell, M. Pettersson, L. Khriachtchev and M. Räsänen, *J. Phys. Chem. A*, 2001, **105**, 3922.
2 A. Kulbida, M. N. Ramos, M. Räsänen, J. Nieminen, O. Schrems and R. Fausto, *J. Chem. Soc., Faraday Trans*, 1995, **91**(11), 1571.

3 R. Fausto, A. Kulbida and O. Schrems, *J. Chem. Soc., Faraday Trans*, 1995, **91**, 3755.
4 M. D. G. Faria, J. J. C. Teixeira-Dias and R. Fausto, *Vib. Spectrosc.*, 1991, **2**, 43.
5 R. Fausto, *J. Mol. Struct.*, 1996, **377**, 181.
6 R. Fausto, *Rev. Port. Quím.*, 1996, **3**, 59.
7 N. L. Allinger, M. P. Cava, D. C. de Jongh, C. R. Jonhson, N. M. A. Lebel and C. L. Stevens, *Organic Chemistry*, Worth, New York, 1976, ch. 23 and 25.
8 N. Selvakumar, B. Y. Reddy, G. S. Kumar and J. Iqbal, *Tetrahedron Lett.*, 2001, **42**, 8395.
9 M. A. Aramendia, V. Borau, C. Jimenez, J. M. Marinas, J. R. Ruiz and F. J. Urbano, *Tetrahedron Lett.*, 2002, **43**, 2847.
10 A. T. Rowland, M. D. Winemiller and M. Sabat, *Tetrahedron Lett.*, 1997, **38**, 1287.
11 H. Tsuge, K. Takumi, T. Nagai, T. Okano, S. Eguchi and H. Kimoto, *Tetrahedron*, 1997, **53**, 823.
12 T. Linker, T. Sommermann and F. Kahlenberg, *J. Am. Chem. Soc*, 1997, **119**, 9377.
13 M. Lounasmaa, J. Miettinen, P. Hanhinen and R. Jokela, *Tetrahedron Lett.*, 1997, **38**, 1455.
14 R. B. Grossman and M. A. Varner, *J. Org. Chem.*, 1997, **62**, 9388.
15 A. Abe, *J. Am. Chem. Soc.*, 1984, **106**, 14.
16 E. Vilaseca, *J. Phys. Chem.*, 1993, **97**, 1684.
17 D. Pitea, F. Gatti and B. Marcandalli, *J. Chem. Soc., Perkin Trans. 2*, 1983, **11**, 1747.
18 V. Migrdichian, *Organic Synthesis*, Reinhold, New York, 1957, vol. 1, ch. 7.
19 S. W. Han and K. Kim, *J. Phys. Chem.*, 1996, **100**, 17 124.
20 A. D. Becke, *Phys. Rev. A*, 1988, **38**, 3098.
21 C. Lee, W. Yang and R. G. Parr, *Phys. Rev. B*, 1988, **37**, 785.
22 S. H. Vosko, L. Wilk and M. Nusair, *Can. J. Phys.*, 1980, **58**, 1200.
23 M. J. Frisch, M. Head-Gordon and J. A. Pople, *Chem. Phys. Lett.*, 1990, **166**, 281.
24 R. Krishhnan, J. S. Binkley, R. Seeger and J. A. Pople, *J. Chem. Phys.*, 1980, **72**, 650.
25 T. Clark, J. Chandrasekhar, G. W. Spitznagel and P. V. R. Shleyer, *J. Comput. Chem.*, 1983, **4**, 294.
26 M. J. Frish, J. A. Pople and J. S. Binkley, *J. Chem. Phys.*, 1984, **80**, 3265.
27 M. J. Frisch, G. W. Trucks, H. B. Schlegel, G. E. Scuseria, M. A. Robb, J. R. Cheeseman, V. G. Zakrzewski, J. A. Montgomery, Jr., R. E. Stratmann, J. C. Burant, S. Dapprich, J. M. Millam, A. D. Daniels, K. N. Kudin, M. C. Strain, O. Farkas, J. Tomasi, V. Barone, M. Cossi, R. Cammi, B. Mennucci, C. Pomelli, C. Adamo, S. Clifford, J. Ochterski, G. A. Petersson, P. Y. Ayala, Q. Cui, K. Morokuma, D. K. Malick, A. D. Rabuck, K. Raghavachari, J. B. Foresman, J. Cioslowski, J. V. Ortiz, A. G. Baboul, B. B. Stefanov, G. Liu, A. Liashenko, P. Piskorz, I. Komaromi, R. Gomperts, R. L. Martin, D. J. Fox, T. Keith, M. A. Al-Laham, C. Y. Peng, A. Nanayakkara, M. Challacombe, P. M. W. Gill, B. Johnson, W. Chen, M. W. Wong, J. L. Andres, C. Gonzalez, M. Head-Gordon, E. S. Replogle and J. A. Pople, *Gaussian 98, Revision A.9*, Gaussian Inc., Pittsburgh, PA, 1998.
28 J. H. Schachtschneider, *Technical Report*, Shell Development Co., Emeryville, CA, 1969.
29 G. Keresztury and G. Jalsovszky, *J. Mol. Struct.*, 1971, **10**, 304.
30 S. B. Lopes, L. Lapinski and R. Fausto, *Phys. Chem. Chem. Phys.*, 2002, **4**, 1014.
31 S. Lopes, L. Lapinski and R. Fausto, *Phys. Chem. Chem. Phys.*, 2002, **4**, 3965.
32 A. J. Barnes, *J. Mol. Struct.*, 1984, **113**, 161.
33 S. Coussan, Y. Bouteiller, J. P. Perchard and W. Q. Zhen, *J. Phys. Chem. A*, 1998, **102**, 5789.